Experimental Study on the Impact of Endoscope Distortion Correction on Computer-assisted Celiac Disease Diagnosis

Michael Gschwandtner, Michael Liedlgruber, Andreas Uhl, and Andreas Vécsei

***Abstract*— The impact of applying barrel distortion correction to endoscopic imagery in the context of automated celiac disease diagnosis is experimentally investigated. For a large set of feature extraction techniques, it is found that contrasting to intuition, no improvement but even significant result degradation of classification accuracy can be observed. For techniques relying on geometrical properties of the image material ("shape"), moderate improvements of classification accuracy can be achieved. Reasons for this somewhat unexpected results are discussed and ways how to exploit potential distortion correction benefits are sketched.**

I. Introduction

Several medical fields and applications exist, in which automated decision support systems and other types of computer-aided technologies based on the analysis of endoscopic imagery have been proposed [1]. Since each endoscopic procedure generates images which exhibit specific characteristics depending on the technique used, the computer systems employed for automated technologies must be designed accordingly. Due to the fact that images taken using a traditional endoscope often suffer from various kinds of degradations [2], in many cases various preprocessing techniques are applied to the imagery (to cope with sensor noise, focus and motion blur, specular reflections, etc. [1]).

A different type of degradation present in endoscopical imagery is a barrel-type distortion due to the wide-angle or fisheye nature of the endoscopic optics'. Since the seminal work on distortion correction for endoscopic images by Haneishi et al. [3], several distortion correction procedures have been applied and developed for this application domain (e.g. [4], [5], [6]).

The aim of distortion correction in endoscopy is manifold. Barrel type distortion is claimed to affect diagnosis [7], since it introduces nonlinear changes in the image, due to which the outer areas of the image look significantly smaller than their actual size. Therefore, the estimation of area or perimeter of observed lesions can be significantly incorrect depending on the position in the image [4], [6]. Another issue arises in virtual endoscopy [5], where the endoscope's position is calculated based on an alignment of the corrected endoscopic video to a rendered 3-D CT image. Any other type of geometrical analysis of the image material such as building 3D models also requires an exact camera calibration [8]. Kallemeyn et al. [9] use distortion corrected arthroscopic images to measure the cyclic cartilage compression during knee movement, where it is absolutely necessary to correct the distortion in order to accurately quantify distances between objects. Finally, it has been mentioned that barrel distortion might "lead to corrupted feature values in texture analysis due to the inhomogeneous magnification" [3] and might also lead to "complications using token matching techniques for pattern recognition" [4]. However, no experimental evidence has ever been given with respect to these latter two assumptions, and also no positive effect of distortion correction with respect to the latter problems has been reported so far. The rationale behind this assumption is illustrated in Fig. 1. Texture patches close to the center of distortion (CoD) matched against patches far away from the CoD might exhibit low similarity due to the compression of the features in the patch close to the edge of the image even though the texture content is similar in reality.

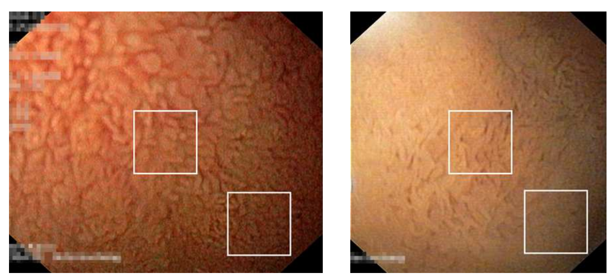

(a) GIF-Q165 (b) GIF-N180

Fig. 1. Texture patches with unequal distance to the CoD

To the authors' knowledge, the potential impact of distortion correction on the analysis of mucosal texture, specifically on the accuracy of corresponding classification techniques has not been addressed so far. In this paper, we apply a classical distortion correction technique described in literature to endoscopic imagery. We compare the classification results achieved in the context of celiac disease diagnosis when classification is applied to duodenal texture patches extracted from original (distorted) images and from distortion corrected images. Section 2 describes the background of applying duodenal mucosa texture classification for diagnosis and staging of celiac disease. In section 3, we describe the experimental setup by first explaining the image database used and the corresponding ground truth. Subsequently, we

Manuscript received June 16, 2010.

Michael Gschwandtner, Michael Liedlgruber and Andreas Uhl are with the Department of Computer Sciences, University of Salzburg, Salzburg, Austria `uhl@cosy.sbg.ac.at`

Andreas Vécsei is with the St. Anna Children's Hospital, Vienna, Austria

This work is partially supported by the Austrian National Bank "Jubiläumsfonds", project no. 12991. The authors acknowledge the help of Sebastian Hegenbart and Georg Wimmer in computing certain feature vectors.

review the classification techniques employed, and finally, the distortion correction technique and its respective application to our image test set are explained. Section 4 presents and discusses experimental results and in section 5 we conclude this work.

II. Automated Classification of Duodenal Texture for Celiac Disease Diagnosis

Endoscopy with biopsy is currently considered the gold standard for the diagnosis of celiac disease. During standard upper endoscopy at least four duodenal biopsies are taken. Microscopic changes within these specimen are classified in histological analysis according to Marsh classification [10].

Automated classification as a support tool is an emerging option for endoscopic diagnosis and treatments (e.g. [1]). In the context of celiac disease, an automated system identifying areas affected by celiac disease in the duodenum would offer the following benefits (among other):

- Methods that help indicating specific areas for biopsy might improve the reliability of celiac disease diagnosis. As biopsying is invasive and the number of biopsy samples should be kept small, optimal targeting is desirable. This targeting can be supported by an automated system for identification of areas affected by celiac disease.
- The whole diagnostic work-up of celiac disease, including duodenoscopy with biopsies, is time-consuming and cost-intensive. To save costs, time, and manpower and simultaneously increase the safety of the procedure it would be desirable to develop a less invasive approach avoiding biopsies. Recent studies [11] investigating such endoscopic techniques report reliable results. These could be further improved by analysis of the acquired visual data (digital images and video sequences) with the assistance of computers.
- The (human) interpretation of the video material captured during capsule endoscopy [12] is an extremely time consuming process. Automated identification of suspicious areas in the video would significantly enhance the applicability and reduce the costs of this technique for the diagnosis of celiac disease.

In first results, the classification of duodenal mucosa texture patches with respect to the prevalence of villous atrophy has been shown to be feasible in principle. Vécsei et al. [13] suggest using histogram-based and wavelet-based features for classification. The same group [14] optimizes Fourier features used for classification by applying an evolutionary process already delivering competitive classification results. In subsequent recent work [15], they have systematically compared the classification performance of two different image capturing techniques and various pre-processing schemes using a set of different feature extraction and classification methods.

III. Experimental Setup

A. Image Acquisition and Marsh Classification

The image test set used contains images taken during duodenoscopies at the St. Anna Children's Hospital using pediatric gastroscopes without magnification (two GIF-Q165 and one GIF-N180, Olympus, with resolution 768×576 and 528×522 pixels, respectively). The main indications for endoscopy were the diagnostic evaluation of dyspeptic symptoms, positive celiac serology, anemia, malabsorption syndromes, inflammatory bowel disease, and gastrointestinal bleeding. The mean age of the patients undergoing endoscopy was 11.1 years (range 0.8-20.9 years). The female to male ratio was 1.43:1. Images were recorded by using the modified immersion technique, which is based on the instillation of water into the duodenal lumen for better visibility of the villi. The tip of the gastroscope is inserted into the water and images of interesting areas are taken. A study [16] shows that the visualization of villi with the immersion technique has a higher positive predictive value. Previous work [15] also found that the modified immersion technique is more suitable for automated classification purposes as compared to the classical image capturing technique. Images from a single patient were recorded during a single endoscopic session and differ by the presented duodenal region only.

There are two duodenal regions with completely different geometric properties, i.e. the Duodenal Bulb and the Pars Descendens. Since the bowel resembles a tube, the chosen perspective considerably changes among images. Textures within images from the Bulbus region lie in the tangent plane to the surface, therefore, the most important distortion is that caused by the endoscopes' optics. The mucosa texture seen within the Pars Descendens region varies between a tangential orientation to a perspective that points out of the surface of the image. Consequently, distortions with respect to texture homogeneity are also caused by differences in perspective in addition to the optics' distortion. Therefore, we concentrate on image material taken from the Duodenal Bulb in this work.

We have created a set of textured image patches with optimal quality to assess if the required classification is feasible under "idealistic" conditions. Thus, the captured data was inspected and filtered by several qualitative factors (sharpness, distortions, visibility of features). In the next step, texture patches with a fixed size of 128×128 pixels were extracted, a size which turned out to be optimally suited in earlier experiments on automated celiac disease diagnosis [15].

In order to generate ground truth for the texture patches used in experimentation, the condition of the mucosal areas covered by the images was determined by histological examination of biopsies from the corresponding regions. Severity of villous atrophy was classified according to the modified Marsh classification in [17]. This histological classification scheme identifies six classes of severity of celiac disease, ranging from class Marsh-0 (no visible change of villi structure) up to class Marsh-3c (absent villi). Since a visible change of the villous structure can be observed at Marsh-3a to Marsh-3c only, we aim at two different classification problems: a four class problem with classes Marsh-0, Marsh-3a, Marsh-3b, and Marsh-3c, and a two class problem with the classes Marsh-0 and Marsh-3 (consisting of images of the latter three classes).

Table I shows the number of images available per considered Marsh-class. As can be seen, for the two class problem the number of images is well balanced, while for the four class problem the Marsh-3 classes contain less images as compared with Marsh-0.

TABLE I
DISTRIBUTION OF IMAGE DATA FROM THE BULBUS DUODENI.

	Marsh-0	Marsh-3a	Marsh-3b	Marsh-3c
#	153	45	54	21

In case only patches close to the CoD would be used during the classification process, the effect of distortion correction with respect to feature sizes together with its potential benefits for texture analysis would be negligible, only artifacts caused by interpolation might degrade the classification result. In order to clarify this, we display the center position of all employed texture patches which have been used in the classification process in Fig. 2.

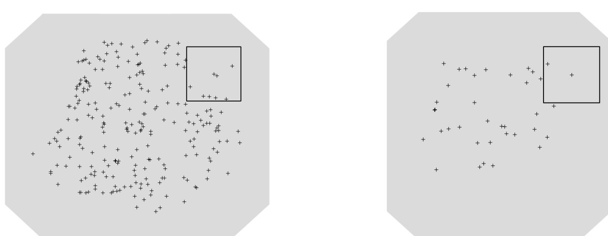

(a) GIF-Q165 (b) GIF-N180

Fig. 2. Distribution of patch centers with one example patch

We note that especially for the GIF-Q165 endoscope, the patches are well distributed (except for the areas where patient related information is overlayed in the upper and lower left corner). For the GIF-N180 endoscope, a rather small number of patches is used overall, but still these are sufficiently well distributed. Obviously it turns out that it is not the case that only patches close to the CoD are involved in our application, so there should be room for classification improvements by distortion correction.

B. Texture Classification Methods

1) Feature Extraction Techniques: To be able to assess the performance of distortion correction techniques with respect to a variety of different classification techniques being applied to corrected imagery, we applied a set of several feature extraction methods that provided the best results in Marsh-based classification of endoscopic image data in earlier work, ranging from transform-based procedures employing FFT or various wavelet transforms to pixel-neighborhood operators like local binary patterns variants. The abbreviations of the techniques used throughout this work are shown in bold (given in alphabetical order):

CWT-Weibull: The Dual-Tree Complex Wavelet Transform is used to decompose the images into 6 scales and the empirical histogram of the detail subband coefficient magnitudes is modeled by two-parameter Weibull distributions. The Weibull parameters are then arranged into a feature vector [18].

Edge-Shapes: After Canny Edge detection, different edge-shape features and texture features of edge-enclosed regions are computed. To find the most discriminative combination of features we use a greedy forward feature subset selection [19]. This technique has originally been developed for colon mucosa pit pattern classification.

ELBP: Extended Local Binary Patterns [20] are used with an 8-neighborhood and scales ranging from 1 to 5. A color version of the image is Sobel filtered using a horizontal and a vertical filter. Optimal filter directions and scales are determined by exhaustive search.

FFT-Evolved: By using the FFT an image is transformed into the respective power spectrum. Multiple ring-shaped filters are then applied to the spectrum of each color channel of the RGB color model to concentrate on discriminative frequency subbands only. Since the number of possible ring filters is quite large, an evolutionary algorithm is used to find an optimal set of filters for each color channel [14]. For each of these ring filters the mean of the coefficient magnitudes within such a ring is used as a feature.

Gabor-Classic: The Gabor Wavelet Transform is used with 4 scales and 6 orientations, the mean and standard deviation of the coefficient magnitudes within a subband are used as features [21].

LBP-Delaunay: First we apply an extended and rotation invariant version of the Local Binary Patterns operator (LBP). The result is used to extract polygons from the images. After computing the Delaunay triangulation we construct histograms from the edge lengths of the Delaunay triangles [19]. This technique has originally been developed for colon mucosa pit pattern classification.

LTP: The Local Ternary Pattern operator [22] is used in an 8-neighborhood to compute histograms for each scale employed (in the range 1 - 5) using a grayscale version of the image. The optimal combination of scales is found by an exhaustive search. The first bin of each histogram is not used.

WT-BBC: The Best Basis Centroids method [23] uses the Best-basis algorithm to find an optimal basis for each image in a training set and computes a centroid over all resulting wavelet packet decomposition structures (maximal decomposition depth 3). After transforming all images into this basis, the most informative subset of the resulting subbands (with respect to a cost function) is used to compute the energy over all coefficients within a subband. These values are concatenated to form the feature vector for an image.

WT-GMRF: This method [24] first transforms an image to the wavelet domain using the pyramidal discrete wavelet transform (two stages) resulting in $3 \cdot 3 \cdot 2 = 18$ detail subbands since we use each color channel of the RGB color model. For each of these detail subbands the Markov parameters of a Gaussian Markov Random Field are estimated. The number of parameters resulting from one detail subband depends on the neighborhood order (neighborhoods used are of Geman type). In addition to the Markov parameters we use the approximation error for each subband as a feature too.

Except for CWT-Weibull and Gabor-Classic, we always pre-processed the images by applying CLAHE [25] followed by a Laplace Sharpening with a kernel size of 9×9 [26].

2) Classification: For classification we apply a k-nearest neighbor (k-nn) classifier to the extracted features to ensure better comparability among the different techniques. In the classifier, all methods except for the LBP-based ones use the Euclidean distance metric for the k-nn classification. The LBP-based methods use the histogram intersection as distance metric. The optimal k-value was determined by exhaustive search through the admissible corresponding parameter range. Based on previous experiences with the different techniques, the parameter range is specified as follows. In case of ELBP, LTP, and LBP-Delaunay k is chosen from 1 to 25 and from 1 to 50 for the Edge-Shape, WT-BBC, and WT-GMRF methods. The results of the FFT-Evolved methods are optimized by an evolutionary process, which either assigns $k = 1$ or $k = 2$ depending on the used chromosomes. The methods DT-CWT-Weibull and Gabor Classic did use a set of k-values ranging from 1 to 10.

The low number of images in our test set does not allow to split the data into training and test set for evaluating classification performance. Therefore, we apply the leave-one-out cross validation (LOOCV) protocol to assess classification accuracy [27]. LOOCV is based on taking a single image of the test set as test image and the remaining images as training data and perform classification. This process is repeated for each single image thus allowing to estimate classification accuracy.

C. Distortion Correction

We use a planar checkerboard pattern (with points on a known grid) for distortion calibration. Calibration points have been extracted manually since we did not want to loose correction precision due to incorrectly determined corner points. Fig. 3 shows two examples of the calibration patterns taken by the two endoscopes (already distortion corrected images are shown).

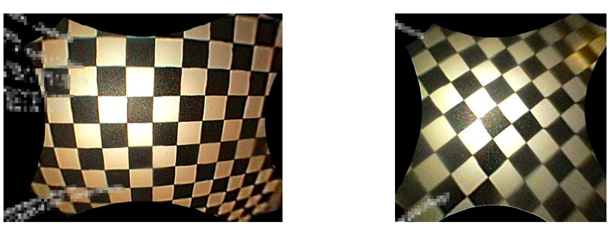

(a) GIF-Q165 (b) GIF-N180

Fig. 3. Distortion corrected calibration pattern taken with both endoscopes

The applied distortion correction technique (DC) relies on the OpenCV software developed by J.-Y. Bouguet (a MATLAB version including extensive documentation and examples is also available[1]). This software is mainly based on the work of Zhang [28]. We extracted 140 calibration points out of 4 images for each of the the GIF-Q165 endoscopes and 144 points out of 4 images for the GIF-N180 endoscope, which were then fed into the software and applied to our images.

As explained in the previous section, the texture patches as counted in table I have been obtained by manually selecting 128×128 pixels sized squares. Since after distortion correction these data do no longer correspond to squares these cannot be used immediately for subsequent classification (most techniques implicitly assume at least a rectangularly shaped texture patch). Therefore we apply the following technique to generate square-shaped texture from distortion corrected image material (which is illustrated in Fig. 4).

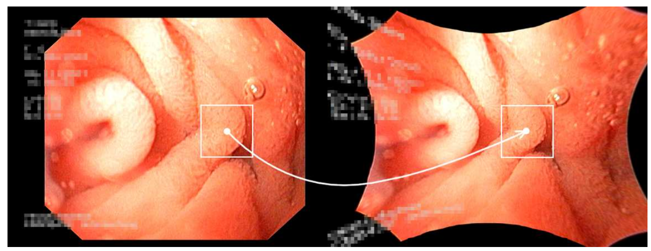

Fig. 4. Generation of distortion corrected texture patches

Based on the original (distorted) endoscopic images, we record the coordinates of the center of the extracted 128×128 pixels. Subsequently, distortion correction is applied to the entire original images and the recorded center coordinates are mapped into the distortion corrected image. Using these coordinates, a 128×128 pixels texture square is extracted from the distortion corrected image which is then used for classification.

Fig. 5 shows examples of original and distortion corrected texture patches which have been generated as described above.

(a) Original (b) DC

Fig. 5. Original and distortion corrected texture patches (Bulbus-set, GIF-Q165 endoscope, class Marsh-0)

IV. Experimental Results

Our results list the classification rates for each Marsh class where Marsh-0 indicates the methods specificity (the percentage of correctly classified images actually showing a normal mucosal state) and the classes Marsh-3a, Marsh-3b and Marsh-3c indicate the methods sensitivity (the percentage of correctly classified images showing villous atrophy).

[1]http://www.vision.caltech.edu/bouguetj/calib_doc/

For simplicity we denote the class Marsh-0 as No-Celiac and the union of all images belonging to Marsh-3a, Marsh-3b and Marsh-3c as Celiac in the two-class case. The *k*-column in the subsequent tables indicates the number of neighbors that were used for the nearest neighbor classification. In order to uniquely identify a specific parameter setting for LBP-based techniques, we use an abbreviation as follows: ELBP$_{HVD135}$, where the digits indicate the scales used and HVD indicates that a horizontally Sobel filtered, a vertically Sobel filtered, and an image filtered in both directions were used for feature extraction, respectively.

TABLE II

2 CLASSES CASE, CLASSIFICATION ACCURACY IN %.

Method	**Classification Results**			
	k	No-Celiac	Celiac	Total
CWT-Weibull	10	97.4	92.5	95.2
DC CWT-Weibull	8	93.5	90.8	92.3
Edge-Shapes	3	94.1	95.0	94.5
DC Edge-Shapes	7	93.4	93.3	93.4
ELBP$_{HV135}$	13	95.4	94.1	94.8
DC ELBP$_{HV135}$	13	93.4	85.0	89.7
FFT-Evolved	1	95.4	96.6	95.9
DC FFT-Evolved	1	95.4	93.3	94.5
Gabor-Classic	4	95.4	90.8	93.4
DC Gabor-Classic	3	93.5	89.2	91.6
LBP-Delaunay	23	78.4	61.6	71.0
DC LBP-Delaunay	9	85.6	56.6	**72.8**
LTP$_{3,5}$	7	99.3	94.1	97.0
DC LTP$_{3,5}$	7	95.4	91.6	93.7
WT-BBC	1	93.4	90.8	92.3
DC WT-BBC	5	92.1	85.8	89.3
WT-GMRF	3	97.3	91.6	94.8
DC WT-GMRF	5	89.5	89.1	89.3

Tables II and III show the results of the different techniques for the two and four classes case, respectively. In the 2 class case, for all but a single classification technique employed, we observe a clear and surprising trend: the overall classification result ("Total" column) is better for the original (distorted) images by about 1.1% (Edge-Shapes) - 5.5% (WT-GMRF) as compared to the corrected images. Only for LBP Delaunay we find an improvement by 1.8%. In the 4 class case (table III) we see similar results. For all but two techniques, distortion correction actually degrades the classification accuracy by 0.7% (ELBP) - 6.3% (WT-GMRF). For two feature extraction techniques we notice an improvement by 0.4%: Edge-Shapes and LBP-Delaunay.

The distribution of good and poor results with respect to different feature extraction techniques is not random. While the results of CWT-Weibull and FFT-Evolved are relatively stable under distortion correction, WT-GMRF is the technique with the largest extent of classification accuracy loss. It seems that the combination of dyadic wavelet transform with coefficient neighborhood modeling is extremely sensitive against the effects of distortion correction as discussed in the next section. Also, LTP and ELTP result in partially significant decrease in classification accuracy.

V. Discussion and Future Work

We have found that assumptions being made in literature turned out to be correct for specific feature extraction techniques only - distortion correction is not able to improve texture pattern matching for the majority of considered feature extraction techniques, at least not in the manner we have set up the system. Interestingly (and this is not unexpected of course), the only two feature extraction techniques relying in some sense on geometrical properties of the images, i.e. Edge-Shapes and LBP-Delaunay, are able to take advantage of distortion correction (for Edge-Shapes improvements are only seen in the 4-class case in fact, however, in the two-class case the amount of accuracy loss is the smallest observed, i.e. 1.1%).

TABLE III

4 CLASSES CASE, CLASSIFICATION ACCURACY IN %.

Method	**Classification Results**					
	k	M-0	M-3a	M-3b	M-3c	Total
CWT-Weibull	10	97.4	57.8	53.7	61.9	79.5
DC DT-CWT-Weibull	14	80.3	28.6	64.2	55.1	78.8
Edge-Shapes	5	95.4	42.2	68.5	61.9	78.7
DC Edge-Shapes	5	94.1	44.4	75.9	52.3	**79.1**
ELBP$_{VD1}$	9	96.7	46.6	68.5	42.8	78.7
DC ELBP$_{HVD123}$	4	94.7	57.7	55.5	57.1	78.0
FFT-Evolved	1	92.8	71.1	75.9	66.6	83.8
DC FFT-Evolved	1	92.1	73.3	68.5	66.6	82.4
Gabor-Classic	4	95.4	66.7	70.4	47.6	82.1
DC Gabor-Classic	3	94.8	55.6	61.1	61.9	79.1
LBP-Delaunay	16	98.6	13.3	12.9	0.0	60.0
DC LBP-Delaunay	6	94.7	26.6	14.8	0.0	**60.4**
LTP$_{135}$	4	99.3	71.1	75.9	61.9	87.1
DC LTP$_{135}$	5	98.0	66.6	64.8	52.3	82.7
WT-BBC	12	97.3	57.7	44.4	57.1	77.2
DC WT-BBC	6	96.7	64.4	48.1	0.0	74.3
WT-GMRF	5	98.0	64.4	66.6	28.5	80.9
DC WT-GMRF	27	94.1	80.0	42.5	0.0	74.3

There are several aspects which may contribute to these somewhat surprising results. On the one hand, the effects with respect to different sizes of texture features caused by the distortion can be at least partially compensated by scale invariance properties of texture descriptors, which are present to some extent in most approaches.

On the other hand, it has to be noted that distortion correction techniques have to apply interpolation especially in the highly distorted areas close to the edge of the image. While for applications that "only" use the distortion corrected image material for navigation purposes or for determination of a lesions size, the values artificially introduced by interpolation techniques do not pose a problem, but they potentially do for texture analysis and feature extraction though. We suspect that artifacts introduced by interpolation might play an important role in the observed classification behavior. This assumption is supported by the fact that techniques relying on the explicit modeling of local pixel neighborhoods (which are severely affected by interpolation of course) like WT-GMRF, LTP, and ELTP are affected most severely by accuracy loss.

An additional problem when comparing the classification results of distorted and undistorted patches is that the shape of the area corresponding to a rectangular patch in the distorted image is no longer rectangular in the distortion corrected one. Therefore, the original and distortion corrected texture patches do not contain exactly the same image material. In order to use identical areas in both "domains" (distorted and distortion corrected) for classification, feature extraction techniques capable of processing arbitrarily shaped texture patches would be required. However, also for the original images, the texture patch is extracted approximately in the region surrounding the area where the corresponding biopsy has been taken so it is by no means guaranteed that the original patches do only contain texture related to a single Marsh class. Therefore, the issue of potential inclusion of small texture areas with different Marsh class in the distortion corrected patches could be considered of minor importance.

In future work, we will investigate the effect of employing different interpolation schemes on the classification results with the aim of achieving distortion correction benefits for a wider class of feature extraction schemes. Additionally, we will refine the analysis of the results by creating statistical information if the probability of misclassifying a patch is somehow correlated to its distance from the CoD in either the distorted and distortion corrected cases. We will also study the effect of applying feature extraction schemes with more explicit scale invariance properties, especially in case patches close to the image edges are involved in classification.

Finally, Barreto et al. [8] have found the parameter-free distortion correction approach of Hartley and Kang [29] being better suited for endoscopic imagery as compared to the classical approach as used in this work. We will investigate the impact of using this approach in our setup.

REFERENCES

[1] M. Liedlgruber and A. Uhl. Endoscopic image processing - an overview. In *Proceedings of the 6th International Symposium on Image and Signal Processing and Analysis (ISPA'09)*, pages 707–712, Salzburg, Austria, 2009.

[2] G. Hanna and A. Cuschieri. Image display technology and image processing. *World Journal of Surgery*, 25(11):1419–1427, 2001.

[3] H. Haneishi, Y. Yagihashi, and Y. Miyake. A new method for distortion correction of electronic endoscope images. *IEEE Transactions on Medical Imaging*, 14(3), 1995.

[4] K. V. Asari, S. Kumar, and D. Radhakrishnan. A new approach for nonlinear distortion correction in endoscopic images based on least squares estimation. *IEEE Transactions on Medical Imaging*, 18(4), 1999.

[5] J. P. Helferty, C. Zhang, G. McLennan, and W.E. Higgins. Videoendoscopic distortion correction and its application to virtual guidance of endoscopy. *IEEE Transactions on Medical Imaging*, 20(7), 2001.

[6] H.-X. Sun, Y.-H. Zhang, and F.-L. Luo. A novel approach for nonlinear distortion correction of industrial endoscope images. In *Proceedings of the 17th World Conference on Nondestructive Testing*, Shanghai, China, 2008.

[7] T. B. Borcharrt, A. Conci, and M. C. d'Ornellas. A warping based approach to correct distortions in endoscopic images. In *Proceedings of the 22nd Brazilian Symposium on Computer Graphics and Image Processing (Sibgrapi 2009)*, Rio de Janeiro, Brazil, 2009.

[8] J. P. Barreto, R. Swaminathan, and J. Roquette. Non parametric distortion correction in endoscopic medical images. In *Proceedings of the 3DTV Conference 2007*, pages 1–4, Kos, Greece, 2007.

[9] N. A. Kallemeyn, N. M. Grosland, V. A. Magnotta, J. A. Martin, and D.R. Pedersen. Arthroscopic lens distortion correction applied to dynamic cartilage loading. *Iowa Orthopaedic Journal*, 27:52–57, 2007.

[10] M. Marsh. Gluten, major histocompatibility complex, and the small intestine. a molecular and immunobiologic approach to the spectrum of gluten sensitivity ('celiac sprue'). *Gastroenterology*, 102(1):330–354, 1992.

[11] G. Cammarota, L. Cuoco, P. Cesaro, et al. A highly accurate method for monitoring histological recovery in patients with celiac disease on a gluten-free diet using an endoscopic approach that avoids the need for biopsy: a double-center study. *Endoscopy 2007*, 39(1):46–51, 2007.

[12] R. Petroniene, E. Dubcenco, and JP. Baker. Given capsule endoscopy in celiac disease: evaluation of diagnostic accuracy and interobserver agreement. *The American Journal of Gastroenterology*, 100(3):685–694, 2005.

[13] A. Vécsei, T. Fuhrmann, and A. Uhl. Towards automated diagnosis of celiac disease by computer-assisted classification of duodenal imagery. In *Proceedings of the 4th International Conference on Advances in Medical, Signal and Information Processing (MEDSIP'08)*, pages 1–4, Santa Margherita Ligure, Italy, 2008. paper no P2.1-009.

[14] A. Vécsei, T. Fuhrmann, M. Liedlgruber, L. Brunauer, H. Payer, and A. Uhl. Automated classification of duodenal imagery in celiac disease using evolved fourier feature vectors. *Computer Methods and Programs in Biomedicine*, 95:S68 – S78, 2009.

[15] S. Hegenbart, R. Kwitt, M. Liedlgruber, A. Uhl, and A. Vécsei. Impact of duodenal image capturing techniques and duodenal regions on the performance of automated diagnosis of celiac disease. In *Proceedings of the 6th International Symposium on Image and Signal Processing and Analysis (ISPA'09)*, pages 718–723, Salzburg, Austria, 2009.

[16] A. Gasbarrini, V. Ojetti, L. Cuoco, G. Cammarota, A. Migneco, A. Armuzzi, P. Pola, and G. Gasbarrini. Lack of endoscopic visualization of intestinal villi with the immersion technique in overt atrophic celiac disease. *Gastrointestinal endoscopy*, 57:348–351, 2003.

[17] G. Oberhuber, G. Granditsch, and H. Vogelsang. The histopathology of coeliac disease: time for a standardized report scheme for pathologists. *European Journal of Gastroenterology and Hepatology*, 11:1185–1194, 1999.

[18] R. Kwitt and A. Uhl. Modeling the marginal distributions of complex wavelet coefficient magnitudes for the classification of zoom-endoscopy images. In *Proceedings of the IEEE Computer Society Workshop on Mathematical Methods in Biomedical Image Analysis (MMBIA'07)*, pages 1–8, Rio de Janeiro, Brasil, 2007.

[19] M. Häfner, A. Gangl, M. Liedlgruber, A. Uhl, A. Vécsei, and F. Wrba. Classification of endoscopic images using Delaunay triangulation-based edge features. In *Proceedings of the International Conference on Image Analysis and Recognition (ICIAR'10)*, Springer LNCS, Povoa de Varzim, Portugal, 2010. to appear.

[20] S. Liao, X. Zhu, Z. Lei, L. Zhang, and S. Li. Learning multi-scale block local binary patterns for face recognition. In *Advances in Biometrics*, pages 828–837. Springer, 2007.

[21] M. Häfner, R. Kwitt, A. Uhl, A. Gangl, F. Wrba, and A. Vécsei. Feature-extraction from multi-directional multi-resolution image transformations for the classification of zoom-endoscopy images. *Pattern Analysis and Applications*, 12(4):407–413, 2009.

[22] X. Tan and B. Triggs. Enhanced local texture feature sets for face recognition under difficult lighting conditions. In *Analysis and Modelling of Faces and Gestures*, volume 4778 of *LNCS*, pages 168–182. Springer, 2007.

[23] M. Liedlgruber and A. Uhl. Statistical and structural wavelet packet features for pit pattern classification in zoom-endoscopic colon images. In P. Dondon, V. Mladenov, S. Impedovo, and S. Cepisca, editors, *Proceedings of the 7th WSEAS International Conference on Wavelet Analysis & Multirate Systems (WAMUS'07)*, pages 147–152, Arcachon, France, 2007.

[24] M. Häfner, A. Gangl, M. Liedlgruber, A. Uhl, A. Vécsei, and F. Wrba. Combining Gaussian Markov random fields with the discrete wavelet transform for endoscopic image classification. In *Proceedings of the 17th International Conference on Digital Signal Processing (DSP'09)*, pages 177–182, Santorini, Greece, 2009.

[25] K. Zuiderveld. Contrast limited adaptive histogram equalization. In Paul S. Heckbert, editor, *Graphics Gems IV*, pages 474–485. Morgan Kaufmann, 1994.

[26] R. C. Gonzalez and R. E. Woods. *Digital Image Processing – Second Edition*. Prentice-Hall, 2002.

[27] K. Fukunaga. *Introduction to Statistical Pattern Recognition*. Morgan Kaufmann, 2nd edition, 1990.

[28] Z. Zhang. A flexible new technique for camera calibration. *IEEE Transactionson Pattern Analysis and Machine Intelligence*, 22(11):1330–1334, 2000.

[29] R. Hartley and S.B. Kang. Parameter-free radial distortion correction with center of distortion estimation. *IEEE Transactions on Pattern Analysis and Machine Intelligence*, 29(8), 2007.